Supporting Information:

Lead-Optimized Design of Metal–Organic Frameworks for Trace SF_6 Capture

Nickolas Gantzler,[a†] *Jackson Geary*[a†] *Jacob A. Harvey,*[a] *R. Eric Sikma*[a] *Raphael A. Reyes*[a] *Caith E. McKeown,*[a] *N. Scott Bobbitt,*[a] *Jason P. Sammon,*[a] *Dorina F. Sava Gallis*[a*]

[a]Sandia National Laboratories, Albuquerque, NM
[†]Co-first author

*Corresponding author: dfsava@sandia.gov

Section S1. Computational Methods and Discussion

1.1. Force Field Benchmarking

The SF_6 FF used in the CoRE-MOF 2019 screening studies by Ren et al.[1] and He et al.[2] was the Straus Optimized model, which treats the SF_6 molecule as a rigid, 7-site model with partial charges.[1, 2] Recently, Matito-Marto et al.[3] fit a rigid, six-site (excludes sulfur), chargeless SF_6 model to experimental vapor-liquid equilibrium (VLE) data in order to study adsorption in hydrophobic zeolites.[3] Both Dellis et al.[4] and Matito-Marto et al. analyze how different models approximate experimental SF_6 vapor-liquid equilibrium data.[3, 4] Notably, the Matito-Marto et al. model performs the best for VLE data, however several "optimized" models from Dellis et al. also closely approximate experimental data.

All the SF_6 models tend to predict the onset of saturation occurring at lower pressure than the experimental data in UiO-66, but many of them predict saturation at a higher pressure than experiments in SBMOF-1.

Overall, most of the models give the closest agreement with UiO-66. For UiO-66, the models converge on a saturation loading of 1.79 mmol/g which is slightly lower than our experimental saturation loading of 2.26 mmol/g (50.8 cc/g at 298 K). These values are in close agreement with previous work buy Kim et al. which reported a capacity at saturation of 1.65 mmol/g at 298 K. [5]

The simulated isotherms in SBMOF-1 don't fully saturate by 100 kPa and exhibit the greatest stratification among the FF models. For example, the Pawley model predicts 1.2 mmol/g and the Matito-Marto model predicts 0.6 mmol/g while the experimental value is 1.02 mmol/g (22.8 cc/g) [6]. The spherical model overestimates the experimental data in SBMOF-1 but most closely captures the shape and onset of saturation. The Strauss Optimized model exhibits little to no adsorption in SBMOF-1 due to its large sigma value relative to the pore diameter. However, given that SBMOF-1 experimentally does adsorb SF_6[6], it may be that the diameter of this model is unrealistically large, resulting in an underestimation of SF_6 adsorption. In UiO-66 and $Ni(ina)_2$, the spherical model is comparable to the Pawley model which comes the closest to reproducing the experimental data.

In UiO-66, the Coulombic contribution to SF_6-MOF fall between 0.09-0.12%. The electrostatic contributions to SF_6-SF_6 interactions are as high as 88% at low pressures for the Strauss Optimized model. However, the SF_6-SF_6 interaction energies are orders of magnitude smaller than the SF_6-MOF interactions, so the adsorption is still governed by SF_6-MOF interactions.

1.2. High-throughput In Silico Screening

High-throughput computational screening has become a popular tool to uncover design principles and winnow candidate pools for discovery and design of MOFs for targeted applications.[7-11] We screened the ARCMOF database using single-component GCMC at 298 K and 1.0 Pa to identify potential high-performing candidates for SF_6 adsorption.[12] The ARCMOF database contains ~ 280k real and hypothetical MOFs compiled from a variety of databases in the literature.

A plot of the single-component uptake vs largest cavity diameter (LCD) is shown **Figure S8**. Only 0.04% of MOFs show an SF_6 uptake of greater than 0.5 mmol/g. There is a sharp, distinct peak in uptake around LCD 5.2 Å, comparable with the kinetic diameter of SF_6. This is consistent with previous observations from other studies. SF_6 adsorption is largely governed by van der Waal interactions and the most important parameter for a MOF with good selectivity is pore size. [1, 2]

The highest performing materials in the in the ARCMOF database are a family of aluminum fumarate MOFs which have been previously reported for SF_6/N_2 selectivity by Li et al..[13,14] These are followed by a series of microporous aluminum phosphates (ALPOs) and a mix of hypothetical MOFs.[15-18] Many of the hypothetical MOFs have esoteric linkers, making synthesis difficult or even impossible. Further, their potential air and moisture stability is of concern, making the pursuit of these materials unfeasible.

SBMOF-1 is among the highest performing candidates with an uptake of 0.87 mmol/g at 298 K and 1.0 Pa [18] and a reported ideal adsorbed solution theory (IAST) SF_6/N2 (1/99) selectivity of 325 [6]. Comparatively, $Ni(ina)_2$ exhibits an uptake of 0.65 mmol/g at 298 K and 1.0 Pa and has predicted IAST SF_6/N_2 (10/90) of 375.[19] Derivatives of $Ni(ina)_2$ have been shown to enhance noble gas selectivity under dilute conditions.[20] Therefore, we pursued $Ni(ina)_2$ and its derivatives for further investigation.

Section S2. Dynamic flowthrough testing

The experimental setup is visualized in **Figure S1**. Briefly, 100mg of the MOF was separately contained within a 3.5x0.25in stainless steel tube (empty thermal desorption tube) with deactivated glass wool containing the MOF on both the inlet and outlet sides of the tube. These tubes were connected to a flow path leading from a Tedlar bag containing neat SF_6, through an Allicat mass flow controller (set for SF_6 flow) into the MOF-containing thermal desorption tube. Viton tubing was used from the Tedlar bag to a Swagelok 1/8-in tubing adapter. Silcotek coated steel tubing was installed between this adapter to the mass flow controller. The MOF tube was attached directly at the outlet of the mass flow controller. Even pressure was applied to the Tedlar bag to force the SF_6 into the flow path. The mass flow controller was set to 1 sccm/min of SF_6 flow. Pressure was maintained on the Tedlar bag for 10 minutes such that 10 sccm of SF_6 was flown through the MOF-containing tube. This setup was used for MOFs $Ni(ina)_2$ and repeated in duplicate. MOF $Ni(ina)_2$ was later repeated in triplicate using a 10 sccm/min flow for 10 minutes, to deliver 100 sccm of SF_6 to the MOF.

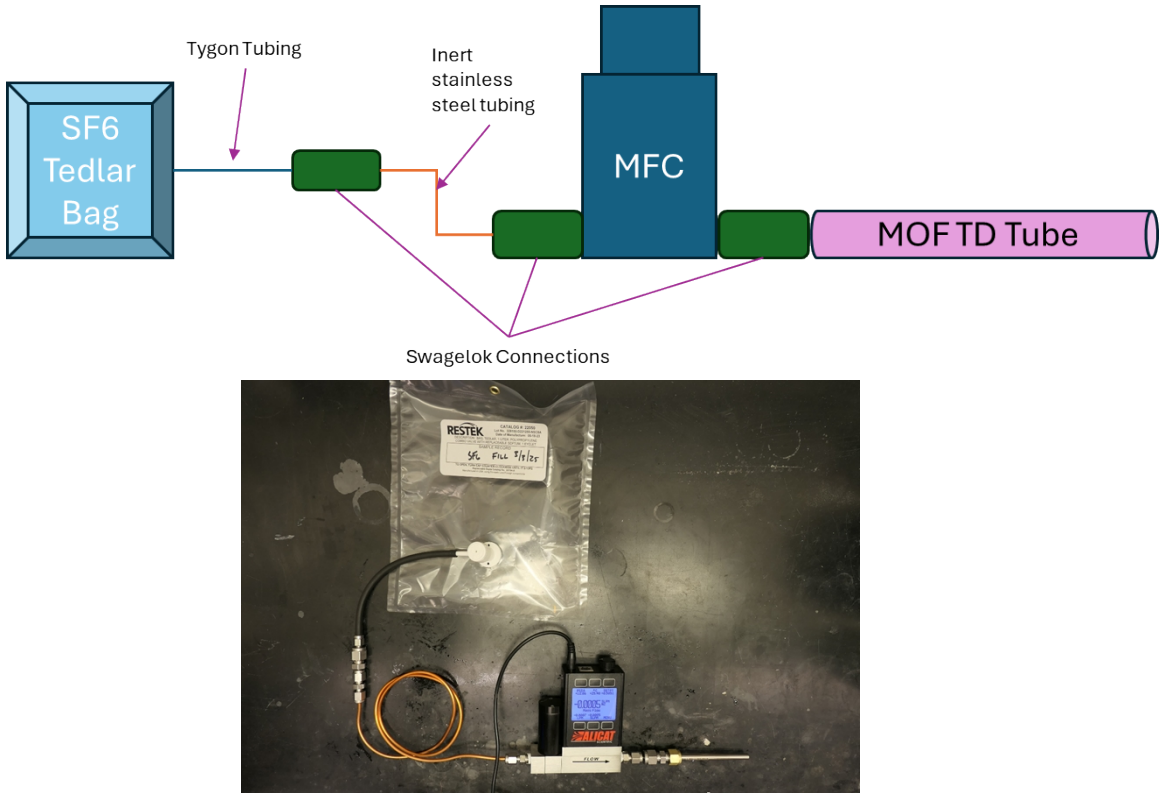

Figure S1 | Schematic diagram of SF_6 testing apparatus and photograph of SF_6 delivery system including Tedlar bag.

Once the requisite flow time was reached, the Tedlar bag output valve was closed, and the thermal desorption tube was removed from the flow path and capped with a Gerstel TD3.5+ analysis cap and installed in a TD3.5 autosampler rack. Analysis of the sample was performed using a LECO GCxGC High Resolution Time of Flight Mass Spectrometer, with a Gerstel TDS 3.5+ coupled with a CIS for sample introduction.

The sample tube was loaded into the Gerstel TD3.5+ Thermal Desorber, and was rapidly heated from 40°C to 150°C at 400°C/min. The vaporous sample was recollected on a cryogenic refocusing inlet maintained at -70°C for the duration of the 5-minute desorption process. Following desorption completion, the cryogenic inlet was rapidly heated at 12°C/sto 300°C and the gas chromatograph run was started. The Gas Chromatograph was maintained at 100°C isothermally for the entire 7-minute analytical run. Inlet Helium pressure was maintained a 4.5 psi under splitless injection conditions. While capable of performing two-dimensional gas chromatography, the LECO system was maintained in a single-dimension mode for this analysis.

The mass spectrometer was set to scan for 50-135 mass to charge ratio (m/z), with the primary m/z fragments for SF_6 being 89 and 127. Data was analyzed visually looking for chromatographic peaks for m/z fragments 89 and 127. Initial tests with 1mL/min for 10 minutes showed a response to desorption from MOF $Ni(ina)_2$ (**Figure S2**). The raw chromatogram shows a response for 89 (orange) and 127 (green) m/z which corresponds to SF_6. The mass spectra stick plot also shows a positive identification for SF6. Similar chromatograms were observed for other replicates of $Ni(ina)_2$ (**Figure S3**).

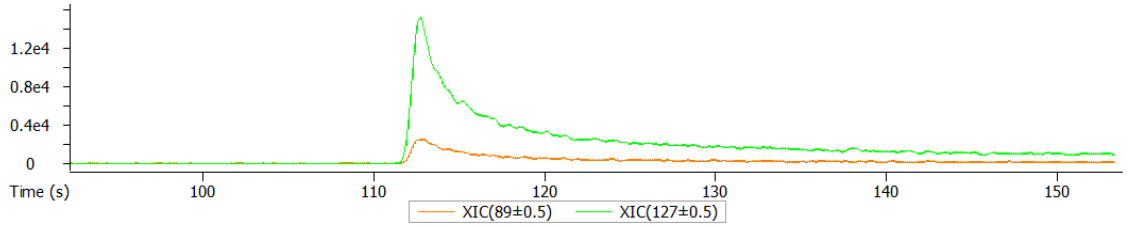

Figure S2 | Chromatograms of desorption for raw SF_6 and $Ni(ina)_2$ showing response for 89 m/z (orange) and 127 m/z (green) corresponding to SF_6.

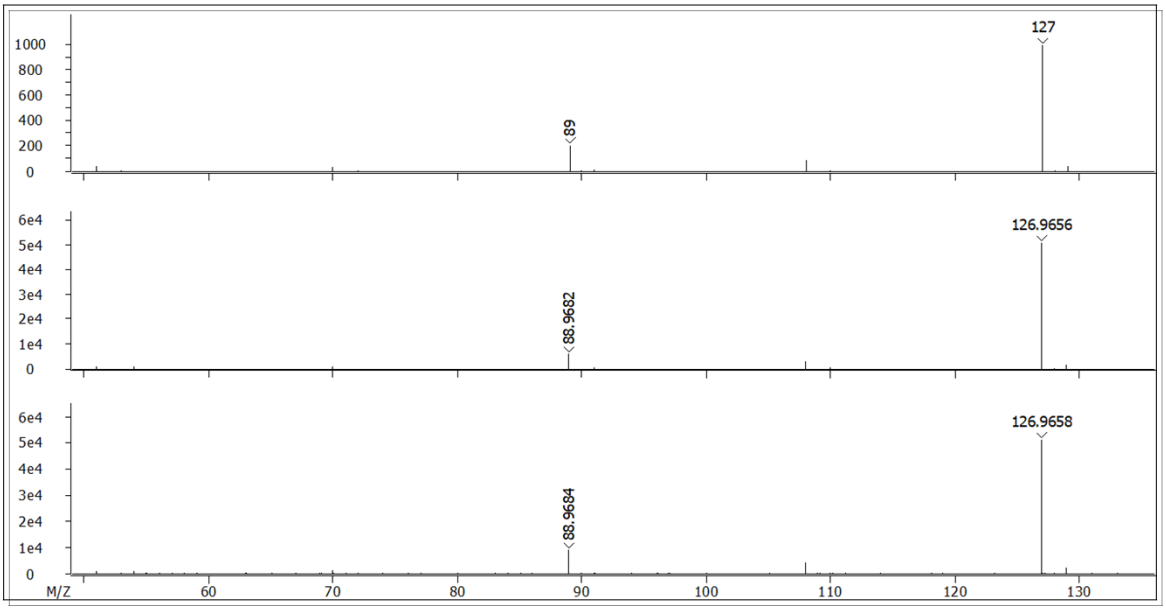

Figure S3 | Desorption replicates for $Ni(ina)_2$.

Following a calibration curve, the raw results were processed against the curve. The **Table S1** below illustrates the mass of SF_6 recovered per mg of MOF.

Table S1 | SF_6 capture data for replicates for $Ni(ina)_2$.

Rep	**Flow Rate (mL/ min)**	**Flow Time (min)**	**Total SF_6 (mL)**	**Mass MOF (mg)**	**Split Ratio**	**SF_6 Area**	**SF_6 Mass (after Split)**	**SF_6 Mass total in sample**	**Mass SF_6 Capture (ug) per mg MOF**
1	1	10	10	96.5	25	3072574	0.100486549	2.512163734	0.026032785
2	1	10	10	96.5	25	3045938	0.100461247	2.511531183	0.02602623

Section S3. Additional Tables and Figures

Table S2 | Physical Properties including the critical temperature, critical pressure, and acentric factor are used in the GCMC simulations for SF_6, Xe, N_2, and CO_2.

Species	**Kinetic Diameter [Å]**	**Normal Boiling Point [K]**	**Polarizability [Å³]**	**T_c [K]**	**P_c [MPa]**	**Acentric Factor**	**Source**
SF_6	5.128-5.2	209.25	4.49 - 6.54	318.7232	3.754984	0.218	21-24
Xe	4.1	165.03	4.005	289.733	5.842	0.00363	22, 24-26
N_2	3.64	77.35	1.17 - 1.74	126.192	3.3958	0.0372	21, 22, 24, 26
CO_2	3.30	194.69	2.507	304.1	7.3773	0.224	24, 26-28

Table S3 | SF_6 molecular FF parameters.

Model	ϵ_F/k_B [K]	σ_F[Å]	ϵ_S/k_B [K]	σ_S[Å]	$q_F[e]$	l_{S-F} [Å]	r_{cut}^* [Å]	**Mix****	**Source**
Pawley	70.60	2.700	-	-	0	1.565	12.8	LB	29
Pawley Opt.	69.82	2.809	-	-	0	1.565	12.8	LB	4
Strauss	30.07	3.300	90.20	3.700	-0.110	1.564	12.8	LB	30
Strauss Opt.	27.02	2.947	165.14	3.228	-0.110	1.564	12.8	LB	4
Kinney	26.27	2.943	151.54	3.405	-0.175	1.561	12.8	GM	31
Kinney Opt.	26.68	2.963	157.33	3.268	-0.175	1.561	12.8	GM	4
7 sites	27.24	2.954	163.89	3.246	0	1.565	12.8	LB	4
Matito-Marto	73.130	2.843	-	-	0	1.565	12.0	LB	3
Olivet	73.13	2.760	-	-	0	1.565	12.8	LB	32
Olivet Opt.	69.82	2.809	-	-	0	1.565	12.8	LB	4
					$K_r = 693.48\ [kJ/mol\ Å^2], r_0 = 1.565$ [Å]				
					$K_\theta = 238.89\ [kJ/mol\ rad^2], \theta_0 = 90°$				

Spherical	$\epsilon/k_B [K]$	σ [Å]	q [e]	r_{cut} [Å]	Mix	Source
	238.89	4.615	0	12.8	LB	[4]

* In cases where the cutoff radius was not given for the model, 12.8 Å was used.
** LB: Lorentz-Berthelot and GM: Geometric Mean

For fluid simulations, $r_{cut} = 6\sigma$ (e.g. 16.2 Å with σ_F^{Pawley}) is a typical choice and was employed by Dellis and Samios [4]; For adsorption in porous media such as MOFs it is often common to use a cutoff radius of 12.8 Å; however, the cutoff radius is usually specified by the force field.

Harmonic spring potential functions for bond length (r) and angle (θ).

$$U_{intra} = \sum_{bonds} K_r(r - r_0)^2 + \sum_{angles} K_\theta(\theta - \theta_0)^2$$

The Lennard-Jones parameters, bonding lengths and angles, and partial charges for the N_2 and CO_2 force fields used in this study [33].

Table S4 | TraPPE FF LJ and Couldombic parameters for N_2 and CO_2.[34]

Type	**Epsilon [k_B]**	**Sigma [Ang]**	**Q [e]**
N	36.0	3.310	-0.482
N_com	0	0	0.964
C	27.0	2.80	0.700
O	79.0	3.050	-0.350

Table S5 | TraPPE bond parameters for N_2 and CO_2.[34]

Type	**length**	**style**
N≡N	1.10	fixed
N≡N_com	0.55	fixed
C=O	1.16	fixed

Table S6 | TraPPE angle parameters for N_2 and CO_2.[34]

Type	**Angle [deg]**	**style**
N≡N_com#N	180	fixed
O=C=O	180	fixed

Table S7 | MOF-SF_6 energy decomposition. Straus Optimized Model.[30]

MOF	**0.1 Pa**			**10.0 Pa**			**1000.0 Pa**		
	Total	**% vdW**	**% coul**	**Total**	**% vdW**	**% coul**	**Total**	**% vdW**	**% coul**
$Ni(ina)_2$	-15397	100.27	-0.27	-546909	100.27	-0.27	-597289	100.27	-0.27
SBMOF-1	-0.22	103.98	-3.99	-40.08	103.55	-3.55	-3828	103.50	-3.50
UiO-66	-151.91	99.87	0.12	-12713	99.87	0.12	-75333	99.90	0.09

Table S8 | SF_6-SF_6 energy decomposition. Straus Optimized Model.[30]

MOF	0.1 Pa			10.0 Pa			1000.0 Pa		
	Total	**% vdW**	**% Coul**	**Total**	**% vdW**	**% Coul**	**Total**	**% vdW**	**% Coul**
$Ni(ina)_2$	-21.44	100.11	-0.11	-18763	100.18	-0.18	-22261	100.18	-0.18
SBMOF-1	0	0	0	0	0	0	-2.28	98.74	1.25
UiO-66	-0.01	11.67	88.25	-8.29	93.49	6.50	-544.49	99.37	0.62

Table S9 | Heats of adsorption based on the SF_6 Pawley FF[29] and the TraPPE model for N_2 and CO_2[34] using Widom insertion.

MOF	Species	Q_{st} [kJ/mol]
$Ni(ina)_2$	SF_6	-53.83
	N_2	-18.26
	CO_2	-29.76
$Ni(ina\text{-}NH_2)_2$	SF_6	-58.81
	N_2	-20.25
	CO_2	-32.17

Table S10 | Dilute selectivity calculated by the ratio of Henry coefficients H_{SF_6}/H_g where g is N_2 or CO_2.

MOF	S_{SF_6/N_2}	S_{SF_6/CO_2}
$Ni(ina)_2$	40712	101.8
$Ni(ina\text{-}NH_2)_2$	84816	1727

Table S11 | Previously reported SF_6 uptake, SF_6/N_2 (1/9) IAST selectivity, and Heat of Adsorption (Q_{st}) for high-performance materials.

Adsorbents	SF_6 Uptake (mmol/g)	IAST Selectivity	Q_{st} (kJ/mol)			Source
			SF_6	N_2	ratio	
Al(fum)	3.00	50139	-35.9	-7.5	4.79	[13]
Al(fum)@2%HPC	2.79	28978	-35.0	-7.4	4.73	[13]
Al(fum)@5%Kaolin	2.80	34409	-37.5	-8.7	4.33	[13]
$Ni(adc)(dabco)_{0.5}$	2.23	948	-47.6	-19.4	2.45	[35]
$Ni(NDC)(TED)_{0.5}$	2.78	750	-34.1	-13.1	2.60	[36]
$Ni(ina\text{-}NH_2)_2$	1.94	325	-58.81	-20.25	2.90	**This work**
$Ni(ina)_2$	2.39	375.1	-33.4	-16.1	2.07	[19]
	2.28	195157	-53.83	-18.26	2.95	**This work**
SBMOF-1	0.89	325	-32.5	15	2.17	[6]
UiO-66-Br_2	0.75	220	-44.3	-	-	[5]
UiO-66	0.82	127.8	-32.1	-	-	[5]
Zeolite-13X	0.99	56.5	-23	18	1.28	[37]

Table S12 | DFT Charge distribution analysis of SF_6 (isolated molecule), SF_6 in $Ni(ina)_2$, and SF_6 in $Ni(ina\text{-}NH_2)_2$.

Atom	**Base SF_6**	**In $Ni(ina)_2$**	**In $Ni(ina\text{-}NH_2)_2$**
F1	-0.238	-0.239	-0.233
F2	-0.250	-0.214	-0.206
F3	-0.245	-0.244	-0.222
F4	-0.245	-0.239	-0.250
F5	-0.245	-0.252	-0.259
F6	-0.244	-0.242	-0.232
S	1.466	1.450	1.450
sum	0.000	0.020	0.048

Table S13 | SF_6 isotherm data in $Ni(ina)_2$ at 298.150 K. Saturation pressure (P_0) is 17,728.827180 mmHg.

Relative Pressure [P/P_0]	**Absolute Pressure [mmHg]**	**Quantity Adsorbed [cm^3/g STP]**
0.00000054	0.009572	0.0555
0.000002689	0.047664	0.8882
0.000006193	0.109794	2.3325
0.000010985	0.194754	4.3964
0.000016787	0.297611	6.9657
0.000021825	0.386937	9.1726
0.000027012	0.47889	11.3888
0.000033435	0.592756	14.1186
0.000038905	0.689737	16.2605
0.000043989	0.779875	18.174
0.000049295	0.873943	20.0093
0.000054265	0.962059	21.6651
0.000107727	1.909877	33.3598
0.000162408	2.8793	39.1021
0.00021641	3.836696	42.4163
0.000274782	4.871556	44.5342
0.000326052	5.780528	45.7384
0.000387774	6.874774	46.7345
0.000444728	7.884504	47.435
0.000503725	8.93045	47.9879
0.0005605	9.937015	48.3882
0.003053201	54.129681	50.3903
0.005656143	100.276779	50.6291
0.00834548	147.955566	50.8334
0.010984384	194.74025	50.97
0.013576755	240.699951	51.066
0.016168563	286.649658	51.142
0.018792303	333.165497	51.1989
0.021395239	379.3125	51.2071
0.024014452	425.748077	51.1933
0.026633086	472.17337	51.2215
0.029228664	518.189941	51.2315

0.031834673	564.391418	51.2139
0.034445113	610.671448	51.2024
0.03707837	657.356018	51.1932
0.039730849	704.381348	51.2039
0.042281819	749.607056	51.1316

Table S14 | SF_6 isotherm data in Ni(ina-NH_2)$_2$ at 298.150 K. Saturation Pressure (P_0) is 17,728.827180 mmHg.

Relative Pressure [P/P_0]	**Absolute Pressure [mmHg]**	**Quantity Adsorbed [cm³/g STP]**
0.000000536	0.009511	0.0553
0.000002721	0.04824	1.2646
0.000005883	0.104306	3.0369
0.000010837	0.192123	5.9743
0.000016913	0.299844	9.2814
0.000021939	0.388949	11.8862
0.00002702	0.479034	14.1274
0.000032311	0.572835	16.6157
0.000040563	0.719127	19.5799
0.000043223	0.766301	20.4418
0.000049008	0.868858	22.1491
0.000055201	0.978653	23.9976
0.000108038	1.915387	32.8505
0.000161233	2.858479	37.2511
0.000216723	3.842239	39.4321
0.000271457	4.812608	40.4911
0.000326029	5.780109	41.1299
0.000390241	6.918508	41.5183
0.000447174	7.927875	41.7058
0.0005054	8.960142	41.8219
0.000561801	9.960078	41.9084
0.003090132	54.784416	42.2341
0.005699981	101.053978	42.3751
0.00835268	148.083221	42.5034
0.010973865	194.553757	42.6212
0.013591259	240.957077	42.7141
0.01617483	286.760773	42.7944
0.01878412	333.020416	42.86
0.021390741	379.232758	42.8995
0.024005804	425.594757	42.9544
0.026622002	471.976868	43.015
0.029240593	518.401428	43.0879
0.031829513	564.299927	43.1218
0.034431125	610.423462	43.1981
0.03705149	656.879456	43.265
0.039662249	703.165161	43.3498
0.042301559	749.957031	43.4422

Table S15 | Experimental SF_6 isotherm data for UiO-66 at 298.150 K. Saturation pressure (P_0) is 7,728.827180 mmHg.

Relative Pressure [P/P_0]	**Absolute Pressure [mmHg]**	**Quantity Adsorbed [cm³/g STP]**

0.000000589	0.010445	-0.0238
0.000003197	0.056678	0.0196
0.000006069	0.107595	0.0708
0.000012048	0.213602	0.1817
0.000017638	0.312699	0.284
0.00002338	0.414492	0.3883
0.000028906	0.512472	0.4883
0.00003458	0.613055	0.5887
0.000040313	0.714701	0.6899
0.00004592	0.8141	0.7887
0.0000515	0.913027	0.8856
0.000057229	1.014608	0.9846
0.00012392	2.196951	2.0832
0.0001791	3.175228	2.9108
0.000236738	4.197095	3.709
0.000293761	5.208033	4.4392
0.000350702	6.217537	5.1217
0.000408204	7.236972	5.7463
0.000464761	8.239667	6.32
0.000521527	9.246055	6.8689
0.000577636	10.240802	7.4179
0.004389313	77.817368	22.2451
0.006480058	114.883827	26.0599
0.009372357	166.160904	30.0278
0.011825923	209.659744	32.7548
0.014526132	257.531281	35.3236
0.017100944	303.179688	37.43
0.019727573	349.746735	39.3364
0.022327228	395.835571	41.0372
0.02494095	442.173798	42.6023
0.027556413	488.542877	44.0403
0.03015697	534.647705	45.3763
0.032779476	581.141663	46.6186
0.03539583	627.52655	47.7882
0.038021703	674.0802	48.8845
0.040582733	719.484253	49.8407
0.043250424	766.779297	50.8519

Table S16 | Digitized SF_6 isotherm (298 K) in SBMOF-1 from Wang et al. [71].

Absolute Pressure [bar]	**Quantity Adsorbed [cc/g STP]**
0.00530504	1.09375
0.00795756	8.75
0.01061008	14.21875
0.018567639	17.28125
0.021220159	17.828125
0.026525199	18.375
0.050397878	19.6875
0.076923077	20.34375
0.100795756	20.671875

0.127320955	21
0.151193634	21.328125
0.175066313	21.4375
0.201591512	21.546875
0.228116711	21.65625
0.25198939	21.765625
0.275862069	21.875
0.302387268	21.875
0.326259947	21.984375
0.352785146	21.984375
0.376657825	22.09375
0.400530504	22.09375
0.427055703	22.09375
0.450928382	22.203125
0.477453581	22.203125
0.50132626	22.203125
0.527851459	22.3125
0.551724138	22.3125
0.575596817	22.3125
0.599469496	22.421875
0.625994695	22.421875
0.652519894	22.421875
0.676392573	22.53125
0.702917772	22.53125
0.726790451	22.640625
0.75331565	22.53125
0.777188329	22.640625
0.801061008	22.640625
0.827586207	22.75
0.851458886	22.75
0.875331565	22.75
0.901856764	22.75
0.925729443	22.75
0.952254642	22.75
0.978779841	22.859375
0.99734748	22.859375

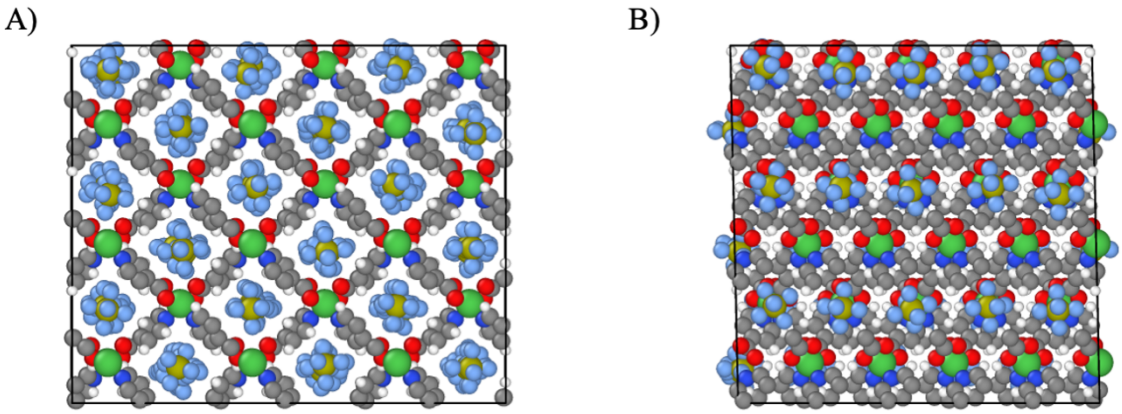

Figure S4 | A GCMC snapshot at 298K and 100 kPa of SF_6 (Pawley FF) in $Ni(ina)_2$ looking (A) down the pores and (B) at a cross section of the 1D pores. The SF_6's form ordered columns in the pores with one SF_6 molecule per binding site.

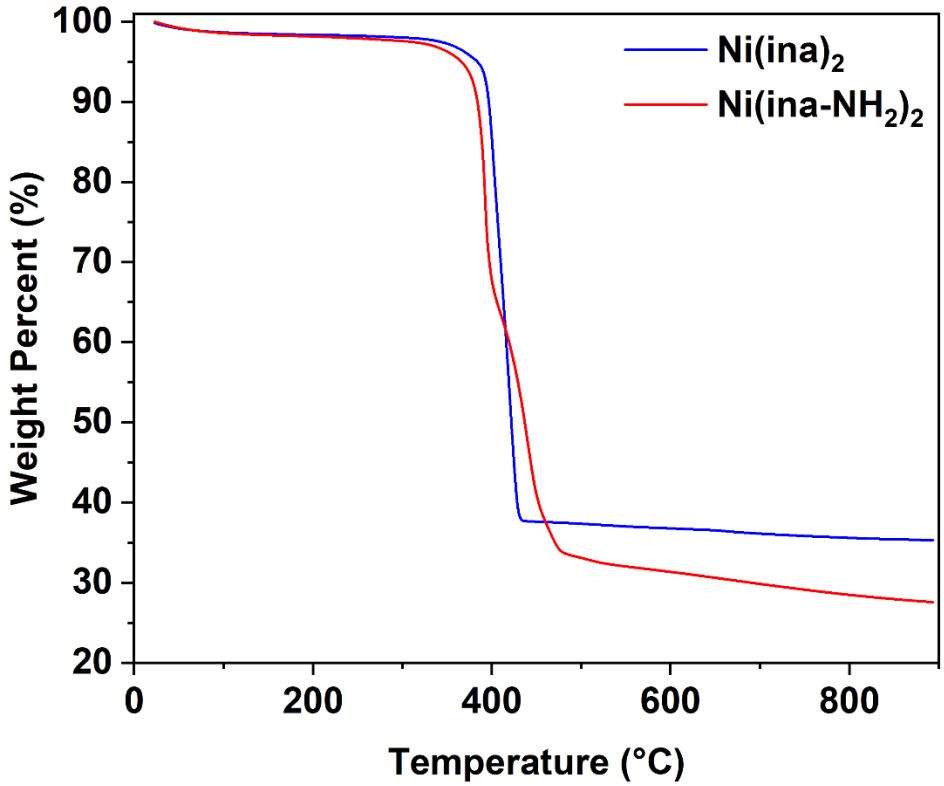

Figure S5 | Thermogravimetric analysis curves under N_2 up to 900 °C for $Ni(ina)_2$ (blue) and $Ni(ina\text{-}NH_2)_2$ (red).

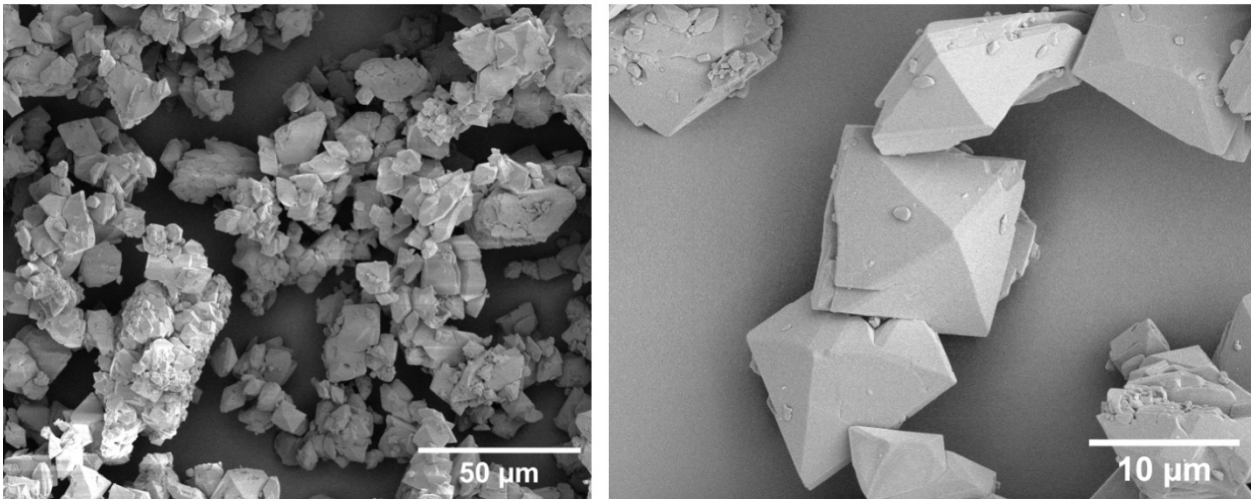

Figure S6 | SEM of $Ni(ina)_2$.

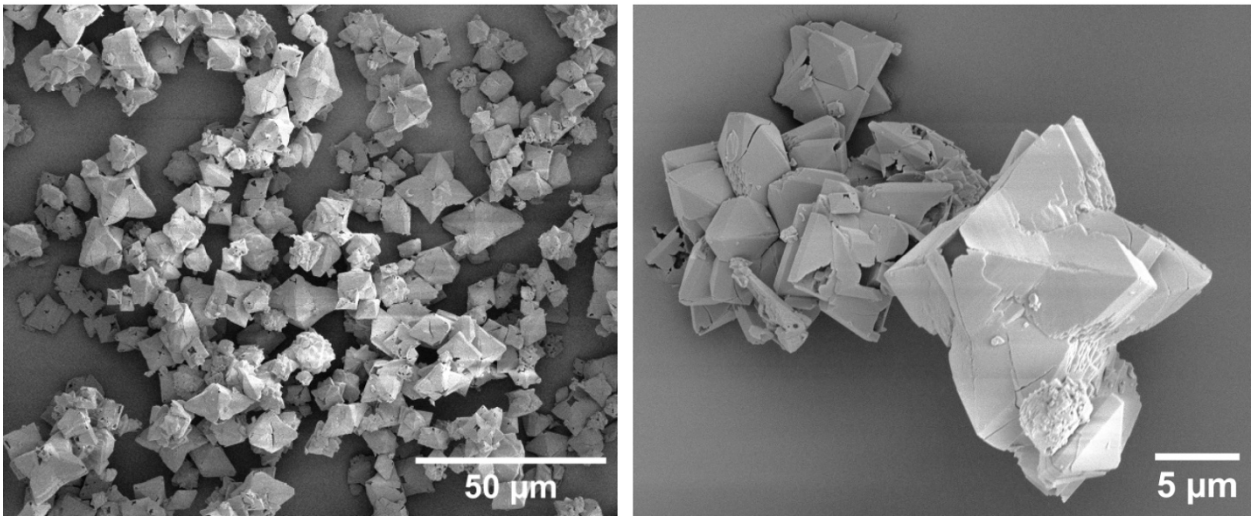

Figure S7 | SEM of $Ni(ina\text{-}NH_2)_2$.

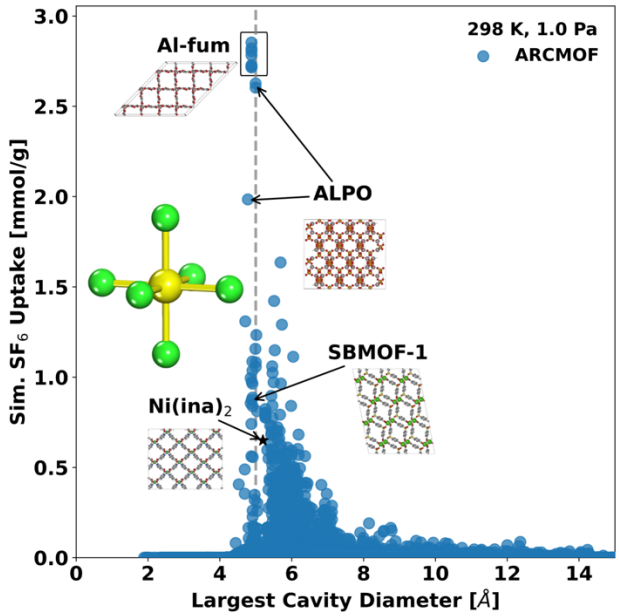

Figure S8 | Simulated SF_6 uptake at 298 K and 1.0 Pa vs. largest cavity diameter (LCD) for the ARCMOF database. $Ni(ina)_2$— not included in database — is among the top 0.04% with uptakes above 0.5 mmol/g. The family of Al-fumarate MOFs is enclosed in a box. Several aluminum phosphates (ALPOs) are indicated as high performing materials. SBMOF-1 is indicated with an arrow. The grey vertical dash represents the kinetic diameter of SF_6 = 5.2 Å. MOFs with LCD's greater than 15 Å are excluded from the plot but generally have very low SF_6 uptake at 298 K and 1.0 Pa.

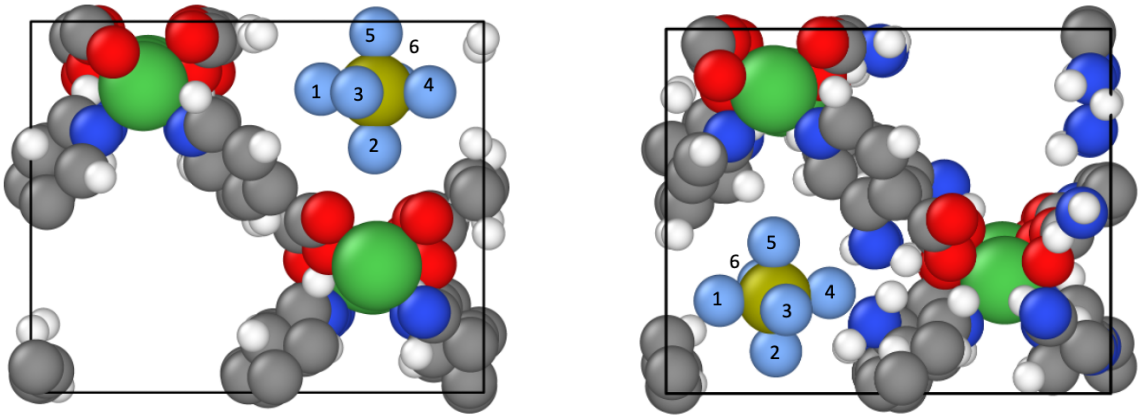

Figure S9 | SF_6 at adsorption site in (left) $Ni(ina)_2$ and (right) $Ni(ina\text{-}NH_2)_2$ for charge distribution calculation.

References

1. J. Ren, M. Chang, W. Zeng, Y. Xia, D. Liu, G. Maurin and Q. Yang, *Chemistry of Materials*, 2021, **33**, 5108–5114.
2. Y. He, X. Cao, Z. Zhang, Z. Jiang, H. Huang, S. Zhang, Q. Han and C. Zhong, *Industrial & Engineering Chemistry Research*, 2023, **62**, 7642–7649.
3. I. Matito-Martos, J. Álvarez-Ossorio, J. J. Gutiérrez-Sevillano, M. Doblaré, A. Martin-Calvo and S. Calero, *Physical Chemistry Chemical Physics*, 2015, **17**, 18121–18130.
4. D. Dellis and J. Samios, *Fluid Phase Equilibria*, 2010, **291**, 81–89.
5. M.-B. Kim, K.-M. Kim, T.-H. Kim, T.-U. Yoon, E.-J. Kim, J.-H. Kim and Y.-S. Bae, *Chemical Engineering Journal*, 2018, **339**, 223-229.
6. T. Wang, M. Chang, T. Yan, Y. Ying, Q. Yang and D. Liu, *Industrial & Engineering Chemistry Research*, 2021, **60**, 5976-5983.
7. A. Sturluson, M. T. Huynh, A. R. Kaija, C. Laird, S. Yoon, F. Hou, Z. Feng, C. E. Wilmer, Y. J. Colon, Y. G. Chung, D. W. Siderius and C. M. Simon, *Mol Simul*, 2019, **45**.
8. Y. J. Colon and R. Q. Snurr, *Chem Soc Rev*, 2014, **43**, 5735-5749.
9. S. Kancharlapalli and R. Q. Snurr, *ACS Appl Mater Interfaces*, 2023, **15**, 28084-28092.
10. Z. Shi, W. Yang, X. Deng, C. Cai, Y. Yan, H. Liang, Z. Liu and Z. Qiao, *Molecular Systems Design & Engineering*, 2020, **5**, 725-742.
11. X. Bai, Z. Shi, H. Xia, S. Li, Z. Liu, H. Liang, Z. Liu, B. Wang and Z. Qiao, *Chemical Engineering Journal*, 2022, **446**.
12. J. Burner, J. Luo, A. White, A. Mirmiran, O. Kwon, P. G. Boyd, S. Maley, M. Gibaldi, S. Simrod, V. Ogden and T. K. Woo, *Chemistry of Materials*, 2023, **35**, 900-916.
13. J. Li, Y. Chen, T. Ke, Y. Jin, R. Fan, G. Xu, L. Yang, Z. Zhang, Z. Bao, Q. Ren and Q. Yang, *Nature Communications*, 2025, **16**.
14. Y. Lan, T. Yan, M. Tong and C. Zhong, *Journal of Materials Chemistry A*, 2019, **7**, 12556-12564.
15. P. G. Boyd, A. Chidambaram, E. Garcia-Diez, C. P. Ireland, T. D. Daff, R. Bounds, A. Gladysiak, P. Schouwink, S. M. Moosavi, M. M. Maroto-Valer, J. A. Reimer, J. A. R. Navarro, T. K. Woo, S. Garcia, K. C. Stylianou and B. Smit, *Nature*, 2019, **576**, 253-256.
16. R. Gurnani, Z. Yu, C. Kim, D. S. Sholl and R. Ramprasad, *Chemistry of Materials*, 2021, **33**, 3543-3552.
17. Y. G. Chung, D. A. Gomez-Gualdron, P. Li, K. T. Leperi, P. Deria, H. Zhang, N. A. Vermeulen, J. F. Stoddart, F. You, J. T. Hupp, O. K. Farha and R. Q. Snurr, *Sci Adv*, 2016, **2**, e1600909.
18. Y. G. Chung, E. Haldoupis, B. J. Bucior, M. Haranczyk, S. Lee, H. Zhang, K. D. Vogiatzis, M. Milisavljevic, S. Ling, J. S. Camp, B. Slater, J. I. Siepmann, D. S. Sholl and R. Q. Snurr, *Journal of Chemical & Engineering Data*, 2019, **64**, 5985–5998.
19. S. M. Wang, X. T. Mu, H. R. Liu, S. T. Zheng and Q. Y. Yang, *Angewandte Chemie*, 2022, **134**.
20. N. Gantzler, M.-B. Kim, A. Robinson, M. W. Terban, S. Ghose, R. E. Dinnebier, A. H. York, D. Tiana, C. M. Simon and P. K. Thallapally, *Cell Reports Physical Science*, 2022, **3**, 101025.
21. D. K. J. A. Wanigarathna, J. Gao and B. Liu, *Materials Advances*, 2020, **1**, 310–320.
22. J.-R. Li, R. J. Kuppler and H.-C. Zhou, *Chemical Society Reviews*, 2009, **38**, 1477.

23. M. Gussoni, M. Rui and G. Zerbi, *Journal of Molecular Structure*, 1998, **447**, 163-215.
24. NIST, Computational Chemistry Comparison and Benchmark DataBase, https://cccbdb.nist.gov/pollistx.asp, 2024).
25. D. Chakraborty, S. Nandi, R. Maity, R. K. Motkuri, K. S. Han, S. Collins, P. Humble, J. C. Hayes, T. K. Woo, R. Vaidhyanathan and P. K. Thallapally, *Chemistry – A European Journal*, 2020, **26**, 12544–12548.
26. T. N. Olney, N. M. Cann, G. Cooper and C. E. Brion, *Chemical Physics*, 1997, **223**, 59-98.
27. A. F. Ismail, K. Chandra Khulbe and T. Matsuura, *Gas Separation Membranes*, Springer, 2015.
28. B. Smit, Reimer, J. A., Oldenburg, C. M., & Bourg, I. C., *Introduction to carbon capture and sequestration*, World Scientific, 2014.
29. G. S. Pawley, *Molecular Physics*, 2006, **43**, 1321-1330.
30. G. Strauss, H. Zweier, H. Bertagnolli, T. Bausenwein, K. Tödheide and P. Chieux, *The Journal of Chemical Physics*, 1994, **101**, 662-671.
31. K. E. Kinney, S. Xu and L. S. Bartell, *The Journal of Physical Chemistry*, 1996, **100**, 6935-6941.
32. A. Olivet and L. F. Vega, *J Chem Phys*, 2007, **126**, 144502.
33. J. J. Potoff and J. I. Siepmann, *AIChE Journal*, 2001, **47**, 1676–1682.
34. J. J. Potoff and J. I. Siepmann, *AIChE Journal*, 2004, **47**, 1676-1682.
35. M. Chang, T. Yan, Y. Wei, J.-X. Wang, D. Liu and J.-F. Chen, *Chemistry of Materials*, 2022, **34**, 9134-9143.
36. M. Yang, M. Chang, T. Yan and D. Liu, *Separation and Purification Technology*, 2022, **295**.
37. M.-B. Kim, T.-U. Yoon, D.-Y. Hong, S.-Y. Kim, S.-J. Lee, S.-I. Kim, S.-K. Lee, J.-S. Chang and Y.-S. Bae, *Chemical Engineering Journal*, 2015, **276**, 315-321.